Heat-activated Plasmonic Chemical Sensors for Harsh Environments

PI: Dr. Michael A. Carpenter
SUNY Polytechnic Institute
Colleges of Nanoscale Science and Engineering

Co-PI Dr. Sang-Hyun Oh
University of Minnesota, Twin Cities
Department of Electrical and Computer Engineering

Contract #: DE-FE0007190

Final Report

Reporting Period Start Date: 9/30/2011
Reporting Period End Date: 9/30/2015

Principal Author: Dr. Michael A. Carpenter

Date Report Issued: December 2015

DOE Award Number: DE-FE0007190

SUNY Polytechnic Institute
Colleges of Nanoscale Science and Engineering
Albany, NY 12203
Phone: 518-437-8667
Fax: 518-437-8603
Email: mcarpenter@sunypoly.edu

Disclaimer

Abstract

A passive plasmonics based chemical sensing system to be used in harsh operating environments was investigated and developed within this program. The initial proposed technology was based on combining technologies developed at the SUNY Polytechnic Institute Colleges of Nanoscale Science and Engineering (CNSE) and at the University of Minnesota (UM). Specifically, a passive wireless technique developed at UM was to utilize a heat-activated plasmonic design to passively harvest the thermal energy from within a combustion emission stream and convert this into a narrowly focused light source. This plasmonic device was based on a bullseye design patterned into a gold film using focused ion beam methods (FIB). Critical to the design was the use of thermal stabilizing under and overlayers surrounding the gold film. These stabilizing layers were based on both atomic layer deposited films as well as metal laminate layers developed by United Technologies Aerospace Systems (UTAS). While the bullseye design was never able to be thermally stabilized for operating temperatures of 500^{o}C or higher, an alternative energy harvesting design was developed by CNSE within this program. With this new development, plasmonic sensing results are presented where thermal energy is harvested using lithographically patterned Au nanorods, replacing the need for an external incident light source. Gas sensing results using the harvested thermal energy are in good agreement with sensing experiments, which used an external incident light source. Principal Component Analysis (PCA) was used to reduce the wavelength parameter space from 665 variables down to 4 variables with similar levels of demonstrated selectivity. The method was further improved by patterning rods which harvested energy in the near infrared, which led to a factor of 10 decrease in data acquisition times as well as demonstrated selectivity with a reduced wavelength data set. The combination of a plasmonic-based energy harvesting sensing paradigm with PCA analysis and wavelength down selection offers a novel path towards simplification and integration of plasmonic-based sensing methods using selected wavelengths rather than a full spectral analysis. Integration efforts were designed and modeled for thermal and mass transport considerations by UTAS which led to the 3D printing of scaled models that would serve as the housing for the alternative energy harvesting plasmonic chemical sensor design developed by CNSE.

Table of Contents

1.0 Executive Summary

The development of zero emissions power stations and active emission control systems of gas turbines, coal powered plants, fuel reformers, gas generators and fuel cell systems presents key research initiatives for the DOE's FutureGen plants. In accomplishing these objectives, there are critical needs to develop cost-effective sensing technologies that can function inside the harsh, high-temperature operating environments envisioned therein. We will tackle these challenges by developing robust nanorod chemical sensors at the College of Nanoscale Science and Engineering (CNSE) and a heat-activated plasmonic source at the University of Minnesota. Goodrich will serve as technical consultants as well as developing methods for packaging the finished device.

Objectives for the study will be focused on the 6 following research areas: **1)** Optical modeling of both nanorod and energy harvesting plasmonic devices **2)** Development of ebeam patterned arrays of Au nanorods embedded in metal oxide matrices with optical responses in the 600 nm to 1200 nm range. **3)** Design and development of a plasmonic energy harvesting light source. **4)** Stability and selectivity testing for the detection of the target gases in the presence of interfering species. Principle component analysis (PCA) will be used to analyze the statistically relevant selectivity characteristics of the sensing array **5)** Development of a single wavelength sensor testing station and **6)** Design of packaging details for the integrated device.

Note: A no cost extension for this program was granted during the last quarter of 2014 and will include an extra years worth of time dedicated to completing further tasks associated with this program. Given that the thermal stability of the bulls-eyes was not able to be demonstrated to achieve energy harvesting as outlined in the original proposal, it was determined that the energy harvesting properties of the embedded gold nanorods themselves was an effective method for enabling emission gas detection under harsh conditions. These techniques will be actively researched in the upcoming year along with efforts to further our understanding of detection methods in gas mixtures, as well as the development of Ag/AgOx plasmonic based materials which have large plasmonic shifts under exposure to redox conditions.

2.0 Disseminated Results

Presentations

1. M. A. Carpenter, "Plasmonic based chemical sensors: Sensitivity, Selectivity and Integration Challenges", Fall MRS, **Invited**, December 2015
2. M. A. Carpenter, "Plasmonics enabled chemical sensors with thermal energy harvesting attributes" Department of Chemical Engineering, University of Connecticut, September 2015 – Invited
3. G. Dharmalingam, M. A. Carpenter, "Investigation of the optical and sensing characteristics of nanoparticle arrays for high temperature applications", SPIE DSS, Sensors for Extreme Harsh Environments II, (May 13, 2015)
4. N. Karker, G. Dharmalingam, M. A. Carpenter, "Thermal stability and energy harvesting characteristics of Au nanorods: Harsh environment chemical sensing", SPIE DSS, Sensors for Extreme Harsh Environments II, (May 13, 2015)
5. M. A. Carpenter, "Harsh environment compatible chemical sensors: plasmonics and electrochemical device principles", SPIE DSS, Sensors for Extreme Harsh Environments II, (May 13, 2015)
6. M. A. Carpenter, "Coupled Plasmonics Enabled Chemical Sensors and Thermal Energy Harvesting Structures", Spring ACS, March 2015, **Invited**
7. M. A. Carpenter, "Harsh Environment Compatible Chemical Sensors: Plasmonics and Electrochemical Device Principles", Department of Chemistry, Union College, NY, **Invited,** (February 2015)
8. M. A. Carpenter, "Coupled Plasmonics Enabled Chemical Sensors and Thermal Energy Harvesting Structures", Fall MRS 2014, **Invited**
9. M. A. Carpenter, "Harsh Environment Compatible Chemical Sensors: Plasmonics and Electrochemical Device Principles", Department of Chemical Engineering and Materials Science, Stevens Institute of Technology, **Invited,** (November 2014)
10. M. A. Carpenter, "Hyperspectral Plasmonics Based Harsh Environment Compatible Chemical Sensors", Spring 2014 ACS Conference, **Invited** (March 2014)
11. M. A. Carpenter, "Hyperspectral Plasmonics Based Harsh Environment Compatible Chemical Sensors", Tsukuba Nanotechnology Symposium, University of Tsukuba, Tsukuba, Japan (2013). **Invited**
12. N. A. Joy, M. A. Carpenter, "Electron Beam Lithographically Patterned Au Nanorods for High Temperature Plasmonic-Based Gas Sensing", Materials Research Society, Fall 2012
13. M. A. Carpenter, "Hyperspectral Plasmonics Based Harsh Environment Compatible Chemical Sensors", Gold 2012 Conference, Tokyo, Japan, September 2012
14. M. A. Carpenter, "Plasmonic Based Harsh Environment Compatible Chemical Sensors", TMS 2012, **Invited,** Orlando, Fl. (March 2012)
15. G. Dharmalingam, N. Joy, B. Grisafe, M. A. Carpenter "Plasmonics based detection of H_2 and CO: discrimination between reducing gases facilitated by material control", Materials Research Society Fall 2012.
16. N. A. Joy, M. A. Carpenter, "Electron Beam Lithographically Patterned Au Nanorods for High Temperature Plasmonic-Based Gas Sensing", Materials Research Society, Fall 2012
17. M. A. Carpenter, "Plasmonic Based Harsh Environment Compatible Chemical Sensors", University of Texas at El Paso, Department of Mechanical Engineering, (2012), **Invited**

18. N. Joy, M. Nandasiri, T. Varga, W. Jiang, V. Shutthanandan, P. Nachimuthu, S. Thevuthasan, M. A. Carpenter "Hyperspectral Plasmonics Based Harsh Environment Compatible Chemical Sensors", Noble Metal Nanoparticles, Gordon Conference 2012.
19. M. A. Carpenter, "Plasmonic Based Harsh Environment Compatible Chemical Sensors", Electrical and Computer Engineering Department, University of Minnesota-Twin Cities, (2011), **Invited**
20. M. A. Carpenter, "Plasmonic Based Harsh Environment Compatible Chemical Sensors", 7th Annual Minnesota Nanotechnology Workshop, University of Minnesota-Twin Cites, (2011), **Invited**
21. M. A. Carpenter, "Plasmonic Based Harsh Environment Compatible Chemical Sensors", Composites at Lake Louise, Calgary, Alberta, (2011), **Invited**
22. N. A. Joy, M. Nandasiri, T. Varga, V. Shutthanandan, W. Jiang, P. Nachimuthu, S. Kuchibhatla, S. Thevuthasan, M. A. Carpenter, "Harsh Environment Plasmonic Sensing Using an Array of Gold-Metal Oxide Nanocomposite Films", Materials Research Society Fall 2011.

Publications

1. Z. Zhao, V. A. Rossi, J. P. Baltrus, P. R. Ohodnicki, M. A. Carpenter, "Ag/AgOx/YSZ redox reaction characteristics and a reversible 200nm plasmonic shift", to be submitted to Journal of Physical Chemistry C, (December 2015).
2. N. Karker, M. A. Carpenter, "High figure of merit hydrogen sensor using multipolar plasmon resonance modes", to be submitted to ACS Nano, (December 2015).
3. N. Karker, G. Dharmalingam, M. A. Carpenter, "Thermal energy harvesting near infrared radiation and accessing low temperatures with plasmonic sensors", Nanoscale, **7**, 17798 (2015).
4. G. Dharmalingam, M. A. Carpenter, "Investigation of the optical and sensing characteristics of nanoparticle arrays for high temperature applications", Proc. SPIE 9491, Sensors for Extreme Harsh Environments II, 949108 (May 13, 2015); doi:10.1117/12.2177572.
5. N. Karker, G. Dharmalingam, M. A. Carpenter, "Thermal stability and energy harvesting characteristics of Au nanorods: Harsh environment chemical sensing", Proc. SPIE 9491, Sensors for Extreme Harsh Environments II, 94910I (May 13, 2015); doi:10.1117/12.2177211.
6. J. P. Baltrus, P. R. Ohodnicki, N. A. Joy, M. A. Carpenter, "Examination of Charge Transfer in Au/YSZ for High-Temperature Optical Gas Sensing", Applied Surface Science, **313**, 19-25 (2014).
7. N. Karker, G. Dharmalingam, M. A. Carpenter, "Thermal Energy Harvesting Plasmonic Based Chemical Sensors", ACS Nano, 8, 10953 (2014).
8. N. A. Joy, M. A. Carpenter, "Optical Sensing Methods for Metal Oxide Nanocomposites", *Metal Oxide Nanomaterials for Chemical Sensors*, Eds. M. A. Carpenter, S. Mathur, A. Kolmakov, Springer, NY, NY (2013)
9. *Metal Oxide Nanomaterials for Chemical Sensors*, Editors M.A. Carpenter, S. Mathur, A. Kolmakov, Springer (2013)
10. N. A. Joy, B. K. Janiszewski, S. Novak, T. W. Johnson. S-H Oh, A. Raghunathan, J. Hartley, M. A. Carpenter, "Thermal Stability of Gold Nanorods for High Temperature Plasmonic Sensing", Journal of Physical Chemistry C, **117**, 11718-24 (2013)

11. N. A. Joy, P. H. Rogers, M. I. Nandasiri, S. Thevuthasan, M. A. Carpenter "Plasmonic Based Sensing Using an Array of Au-Metal Oxide Thin Films", Analytical Chemistry, **84**, 10437 (2012).
12. G. Dharmalingam, N. A. Joy, B. Grisafe, M. A. Carpenter, "Plasmonic Based Detection of H_2 and CO: Discrimination Between Reducing Gases Facilitated by Material Control", Beilstein Journal of Nanotechnology, **3**, 712 (2012).

Patents/Technology Disclosures

1. M. A. Carpenter, "Thermal Energy Harvesting Based Chemical Sensors", Provisional patent filed (June 2015)

Student Graduates

Dharmalingam, Gnanaprakash, PhD Estimated May 2015 - CNSE
Nicholas Joy, PhD May 2013 - CNSE
Timothy Johnson, PhD August 2013 – University of Minnesota

3.0 Methods

3.1 Ebeam patterning of nanocomposite samples

A key task for this program was development of methods to not only pattern the plasmonically active nanoparticles but to keep them stable under the sensor testing conditions which could range between 500 and 700C in the presence of oxidizing and reducing gases. The fabrication procedure is outlined as follows. A quartz substrate was cleaned by sonicating in acetone for several minutes and blown dry. A 65 nm base layer of YSZ was then deposited by RF magnetron physical vapor deposition (PVD) using a 99.9% pure YSZ (5 wt% Y_2O_3) target in an ~2 mTorr Ar process pressure. The sample was then annealed at 970 °C for 3 hours in Ar. PMMA 495 A2 was used as the positive electron-beam resist and spin coated on the YSZ base layer at 2000 rpm for 60 seconds. The sample was then baked on a hot plate at 180 °C for 60 seconds resulting in a resist thickness of approximately 70 nm. This was followed by deposition of a 20 nm Cr layer using electron-beam evaporation. Since quartz is non-conducting, the purpose of the Cr layer was to eliminate charging during the EBL write process. Patterning of the rod features was done on a Vistec VB300 Gaussian EBL tool operating at 100 kV. The beam current was set to 5 nA, which yields a theoretical spot size of approximately 7 nm. The exposure dose was set to 1100 μC/cm^2 with a beam step size (pixel size) of 5 nm. After the exposure, the Cr layer was chemically etched away and the PMMA developed using methyl isobutyl ketone and isopropyl alcohol (1:3). Next, 6 nm of Ti followed by 20 nm of Au was deposited by electron-beam evaporation without breaking vacuum between the two depositions. Lift-off of the remaining PMMA was done in boiling acetone leaving the Ti/Au rods on the YSZ surface. A final 15 nm capping layer of YSZ was deposited by PVD using the same conditions as described above. The patterned samples are annealed in in 100 °C steps, from 300 °C to 600 °C, with 6 hours at each temperature, and then followed by cooling to ambient temperatures. The above process steps were used for patterning

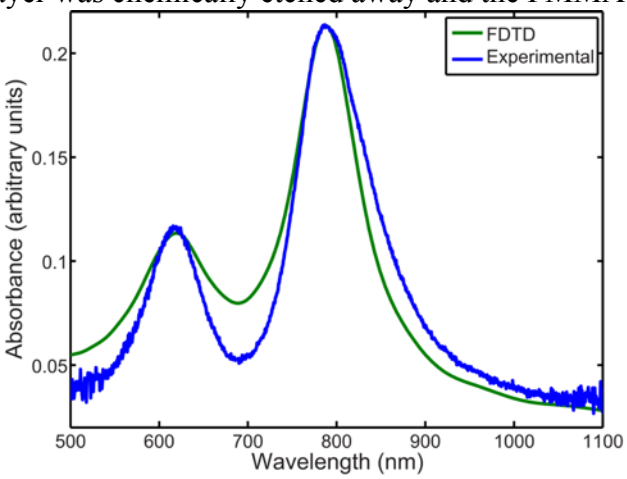

Figure 1. Experimental and simulated absorbance spectra from the array of AuNRs. The experimental spectrum was taken at room temperature after the final 600 °C anneal, but before the start of gas exposures.

Typical experimental absorbance spectra for a sample patterned and annealed in the above fashion can be seen in figure 1. The absorbance spectrum from FDTD modeling is compared to the sample spectrum in Figure 3. Modeling of the transverse and longitudinal absorbance peaks has been performed by the finite-difference time-domain (FDTD) method using full 3-D FDTD simulations in order to verify the origin of the resonances. The simulations were done with a commercial software package (Fullwave, RSoft Design Group) and contained two nanorods with periodic boundary conditions to simulate an infinite array. A pulsed wave was incident from above the nanorods and transmitted power was collected below the rods and then Fourier transformed to obtain the transmission spectra. Simulations were done with both TE- and TM-polarized light and the results were averaged to simulate unpolarized light. Incremental changes in both the length and width of the rods were made and correlated to shifts in peaks of the spectra. Grid sizes of 1

nm were used in the in-plane dimensions while a grid size of 10 nm graded down to 1 nm at the nanorod were used in the dimension perpendicular to the substrate. The optical constants used for Au were originally from Palik and then fit to a Lorentz/Drude model by Rakic[1]. In order to match both the transverse and longitudinal peak positions, the rod width was set to 50 nm (estimated from post-anneal ESEM), and the length was adjusted to 85 nm. It was also necessary to decrease the refractive index of the YSZ to n = 1.53, which serves as an approximation for the effective dielectric constant immediately surrounding the nanorods.

To confirm that the plasmonic spectra pertain to Au nanorods we obtained ESEM images of the sample after the afore-mentioned deposition and annealing process steps. Representative ESEM images are displayed in Figure 2a and 2b for the patterned rods and from rods imaged after annealing at 600^{o}C. It is clear from these images that the patterned rods are able to maintain their respective geometric shape. Critical to the stability is to encapsulate the rods in an overcoating of the metal oxide, which needs to be at least 10nm thick. Rods without any capping layer change to spheres during the annealing process at temperatures of around 350-400^{o}C. Close inspection of Figure 2b notes that there are voids in the patterned rods after the annealing conditions. While these voids do not affect the obtained spectra to any significant degree, a thicker metal oxide overcoat, at least 60nm, minimizes the formation of the voids.

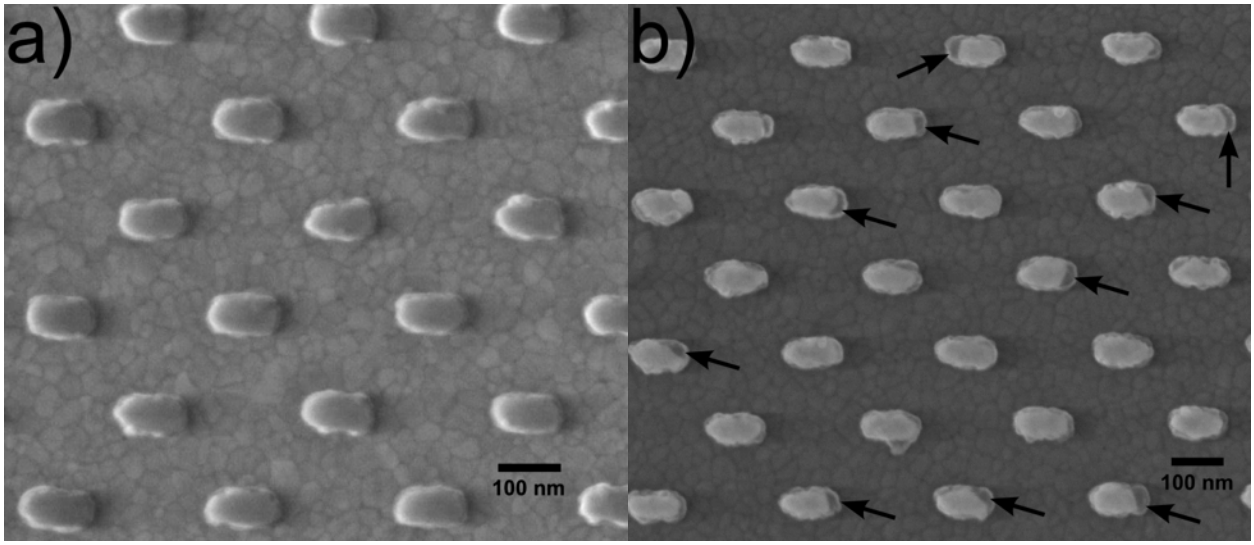

Figure 2. Plan view ESEM images of the AuNRs, a) prior to capping with YSZ or annealing, b) after capping with YSZ and annealing to 600 °C. Arrows point to spots where the Au has separated from the YSZ capping layer as a result of annealing.

3.2 Design and development of plasmonics energy harvesting light source

The aim of the proposed work was to develop energy harvesting bullseye patterns that would absorb thermal energy and emit light at wavelengths specific to to the pitch and width of the rings in the pattern.[2,3,4,5] The schematic in Figure 3 notes that the energy harvested by the bullseyes would be passed through the arrays of plasmonic nanorods with selected wavelengths of light detected as a function of gas exposures for detection of the target gases. Critical to this design is the thermal stability of the nanorods, demonstrated in the previous section, as well as the thermal stability of the bullseye patterns. Stability of these patterns was attempted through both the use of atomic layer deposited metal oxide overcoatings as well as proprietary barrier layers and laminating layers deposited by UTAS (Goodrich is now named United Technologies Aerospace Systems).

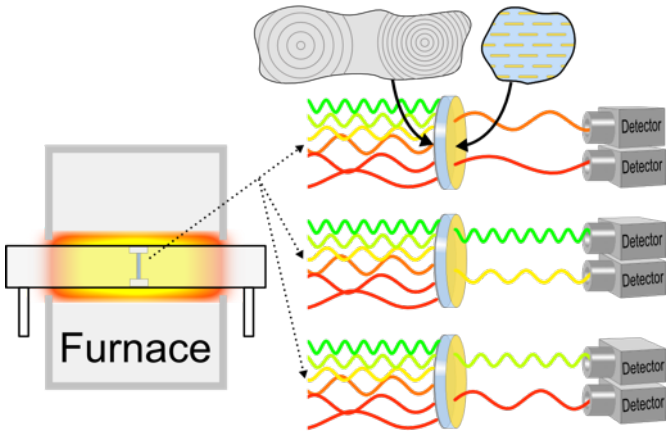

Figure 3: Schematic showing the proposed bullseye energy harvesting scheme with selected wavelengths used for detection

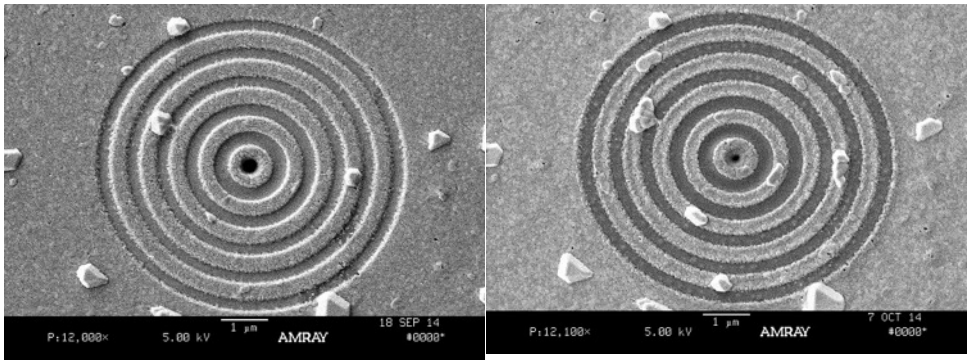

Figure 4: Representative bullseye patterns created using FIB based methods. Left: before annealing, Right: after annealing

Throughout all of the bullseye patterning and stability testing it was determined that the optical quality (dependent on the stability of the bullseye pattern) was not sufficient and began to fail at temperatures as low as 400°C. The patterns shown in Figure 4 are representative of the findings with the pattern on the left being the as deposited bullseye and the pattern on the right being obtained after annealing the sample in a non-reactive gas at 400°C. It is clear that given the surface roughness and particle counts even before annealing that the optical quality will not be sufficient, but comparison with the post anneal shows that the bullseye is actively changing and therefore will not have the necessary stability. Optical reflectance spectra were obtained, but did not show a narrow reflectance peak, expected of the design, and this also changed during the anneal. It was therefore determined that the bullseye design would have to be changed and an alternative to this energy harvesting scheme was necessary.

3.3 Alternative Energy Harvesting Design

As an alternative to using emission from a bulls-eye as a thermally activated light source for probing the plasmonic properties of Au nanorod arrays we have been investigating the potential for the nanorods themselves to be the active light harvester and sensing layer. At above 600˚C, the thermal radiation emitted by the furnace is strong enough in the visible region of the spectrum that the thermal radiation is harvested by the 44x145nm sized gold nanorods embedded within YSZ, thereby enabling an absorbance measurement experiment to be performed. Key to these studies was to modify the test bench as shown in Figure 5, which simply required replacing the white light source, previously used for all absorbance spectra obtained to date, with a mirror. The mirror in these studies allows for more of the thermal radiation to pass through the nanorod sample and enables a demonstration of the thermal harvesting methodology. The thermal energy emitted by the furnace is used as a reference by the CCD and is imaged through an uncoated portion of the quartz substrate. The thermal energy absorbed by the embedded nanorods is then measured and calculated using the CCD imaging detector.

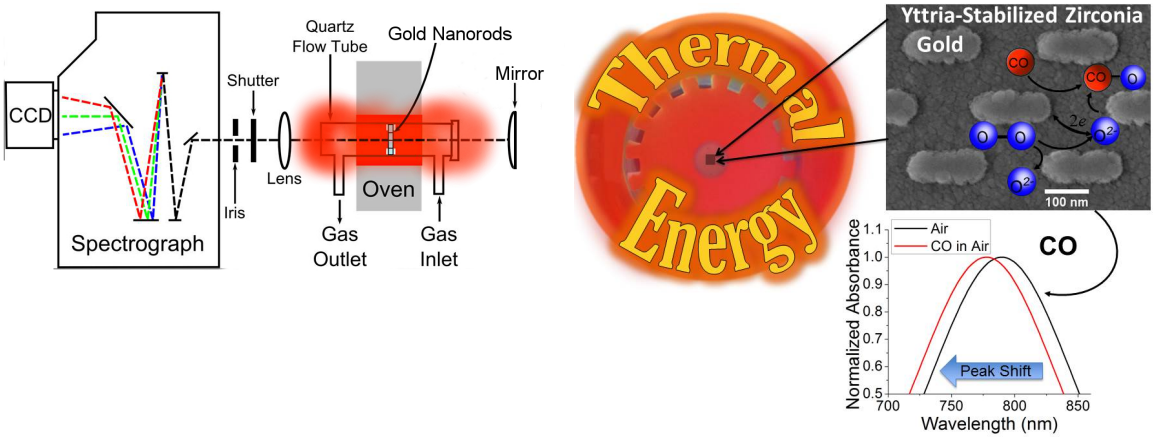

Figure 5: a) Schematic of the thermal imaging bench setup (left). b) Diagram showing the placement of the sample in the macor holder inside the furnace (right). Interfacial surface reactions between CO and oxygen species are also shown.

The initial target gas exposure experiments using this new thermal energy harvesting approach were performed with H_2 mixtures in air with a sample temperature of 500^{o}C. For comparison a standard white light experiment was also performed to ensure that the two data sets were consistent. The data displayed in Figure 6 show the peak position of the plasmon band as a function of time and H_2 concentration in an air carrier gas, both for the thermal energy harvesting data (left) and that of a classic white light experiment(right). The white light experiment used a white light source to probe the plasmon band of the nanorods and was historically how all of the previous data has been obtained. The data quality in Figure 6 appears to be as good as that that has been previously published and reaffirms the quality and methodology of the thermal energy harvesting experiment.

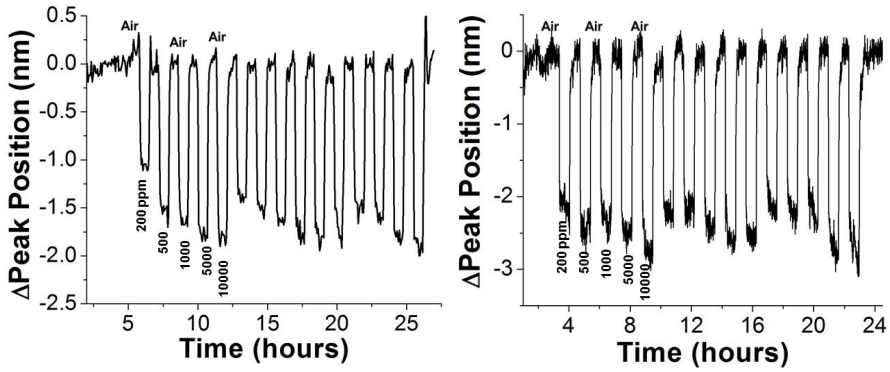

Figure 6: Sensing results for air-H_2 mixture. H_2 concentrations: 200, 500, 1000, 2000, 10000ppm. Thermal imaging data (left), White light data (right).

Beginning in mid 2014 all of the energy harvesting data and sample testing for this demonstration were completed using this alternative approach.

3.4 Sensor Materials Testing

The sample array testing is completed by either mounting individual samples assembled in to a Macor sample holder, including the blank, or by having multiple nanorod array patterns all deposited on an individual quartz substrate. The sample holder is mounted in a quartz flow tube as shown in Figure 7. The flow tube allowed for gas flow during exposure cycles, temperature control from the surrounding furnace, and light transmission for the spectroscopy measurements. A quartz tungsten halogen light source with a UV filter illuminated the samples. On the other side of the flowtube a 75 mm diameter lens with 60

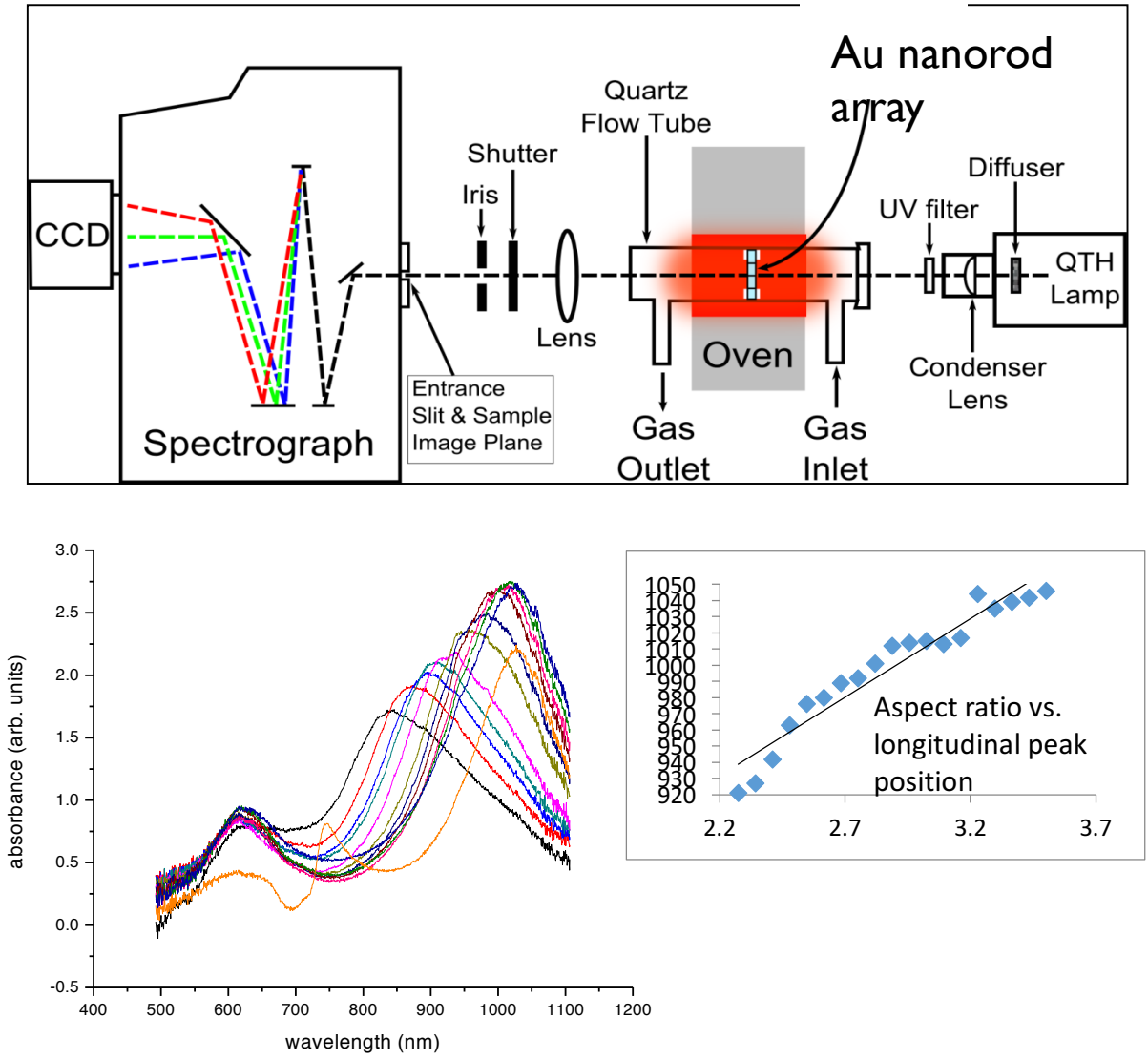

Figure 7: Top: Schematic showing optical hardware used to collect the sensing array data from patterned nanorod samples Left: Absorbance spectra from a 12 element nanorod sensing array all acquired simultaneously using the CCD detection scheme. Right: Plot showing the linear relation between the longitudinal plasmon peak position as a function of aspect ratio

mm focal length was placed 20 cm from the samples, which was used to focus an image of the samples onto an imaging spectrograph after going through a shutter and aperture. An Oriel Instruments MS257 spectrograph and Peltier cooled CCD detector allowed for vertical spatial resolution of the sample image from a 10 μm slit width on the image plane. Absorbance spectra from each of the thin films came from software-defined regions of interest with the blank substrate used as a reference. All gas exposures took place at a temperature of 500°C. Computer controlled mass flow controllers were used to set the various gas concentrations used in the studies for the H_2, CO and NO_2 in air gas mixtures with a constant 2000 sccm flow rate. For all of the experiments with the nanorod samples both the transverse dipole peak and the longitudinal dipole peak positions were monitored as a function of time through collection of the full absorbance spectrum from these samples every 30 seconds during the experiments. A subset of this sensing data can be seen in Figure 8 for the individual nanorod sample described Figures 1 and 2. From the data noted in Figure 8 it is clear that the longitudinal peak is more sensitive than the transverse peak in accordance with previous work using nanorods as biosensors in liquid environments.[6]

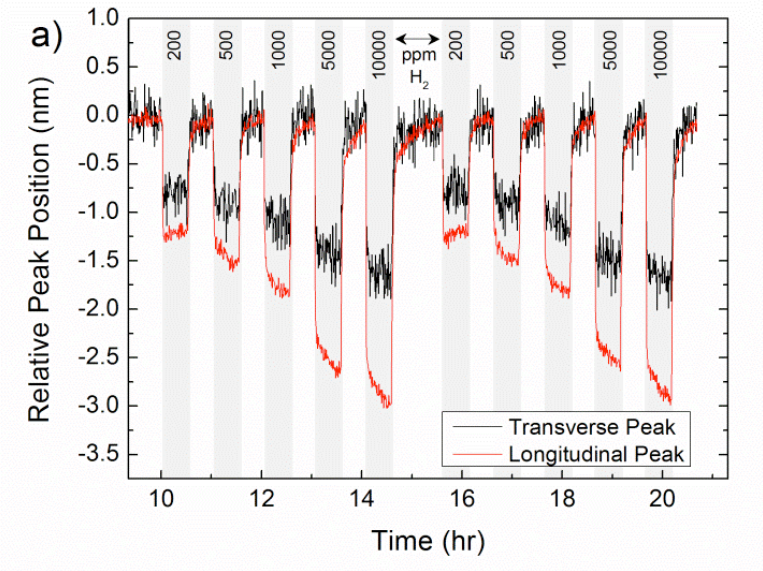

Figure 8: H_2 sensing data for both the transverse and longitudinal dipole plasmon peaks of the sample displayed in Figures 1 & 2.

Extensive array measurements to determine and compare the sensing properties between nanorods patterned in a 12 element sensing array were attempted. While each individual array element responded reliably, what was not possible was to correlate the sensing properties as a function of aspect ratio. This study was undertaken as the trends should have shown that higher aspect ratio rods would be more sensitive. However an interesting point of note, which complicated a determination of sensitivity trends with respect to aspect ratio, is that the fine structured surface detail on the rods within any given array appears to change with time. This is highlighted in Figure 9 where we have obtained ESEM images of a given set of nanorods prior to a 12hr experiment at 500C with alternating H_2/ air and air gas cycles.

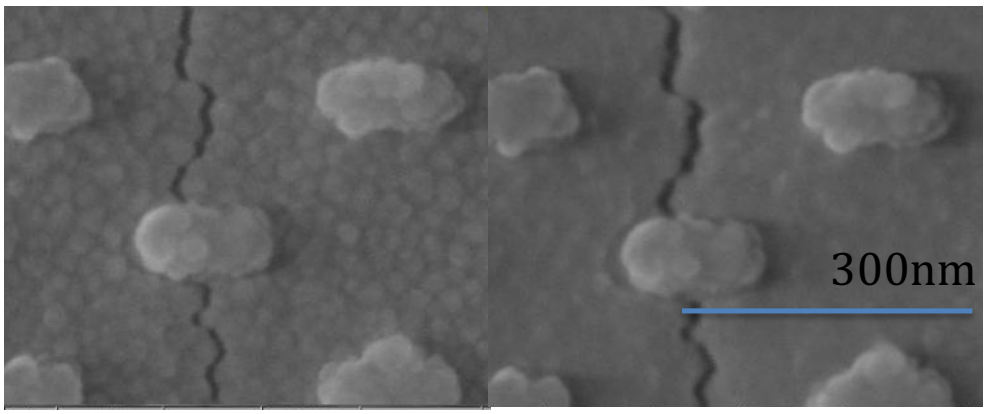

Figure 9: ESEM images of Au-YSZ nanorods before (left) and after (right) a 12hr experiment with alternating air and air/H_2 gas cycles at 500^{o}C.

While Figure 9 only shows a small subset of the rods imaged before and after this exposure experiment, large quantities of rods imaged had similar subtle changes in their surface structure. In Figure 9 the nanorod in the upper right side of each respective image has subtle but relevant changes in its surface features, which are noted by a change in the lobe of gold on the left side of the rod changing, and the right side of the rod showing more well defined edges and nodules after the 12 hr experiment. Quantifying these changes is not possible, but in the scientific literature it is well accepted that the specific facets and surface structure on AuNPs can dramatically alter the reaction cross sections for CO oxidation reactions, as well as hydrocarbon related catalytic reactions. For this particular program, the impact of this study was that a detailed determination of sensing sensitivity as a function of nanorod aspect ratio was not possible as the fine structure of each of the rods appears to be dynamically changing with time at relevant temperatures and gas exposures In terms of matching individual nanorods for optimal use with thermal energy harvesting sensing designs there is no impact at all, as any individual rod that is patterned appears to respond well and reliably, it is their comparative sensing properties across an array that will need to be done experimentally with only coarse design rules with respect to general size and thickness being possible.

4.0 Selectivity Measurements and Development

While sensitivity is difficult to compare given the dynamically changing surface facet structure, as long as the rods are stable during the measurement window selectivity can be characterized. The selectivity measurements are dictated by performing extensive sensor exposure experiments for the target gases which collect the plasmon absorbance spectra every 30s during the exposures. A method of data analysis that has shown great promise in providing the necessary information for analyte gas discrimination using the above principle is principal component analysis (PCA). PCA performs dimensional reduction by generating PC vectors that are linear combinations of the original input variables. The PC vectors lie in directions of maximum variance in the data and are orthogonal to each other. Projection of a combination of principal components onto a subspace is known as a scores plot. The scores plot of the first several principal components usually describes most of the variance present in the data. A representative result of this analysis can be seen for the PCA work completed for both the white light and the thermal imaging data (Figure 10) using the difference spectra obtained from subtracting the LSPR gas-on spectrum from the LSPR gas off spectrum (both spectra were first fitted using the same polynomial routine noted above to reduce random variances in the data set and then smoothed using the Savitzky-Golay algorithm) followed by autoscaling pre-processing for each of the concentrations used in the H_2, CO and NO_2

experiments. Subtraction of the gas spectra was done after completion of the experiment as a separate step in the data analysis. The difference spectra were limited to the wavelength region between 600-1000nm in order to cut out the regimes where noise was dominant, which would negatively influence the PCA analysis. The resulting PC scores plot is displayed in Figure 10 for both the white light and thermal imaging experiments.

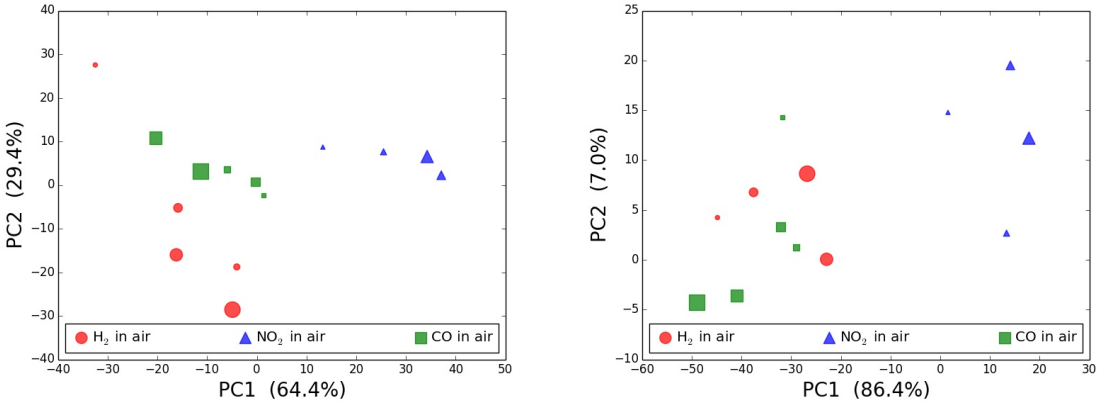

Figure 10. White light full spectrum PCA (left) and thermal imaging full spectrum PCA (right).

The white light data shown in Figure 10 shows a unique gas response for the three analyte gases. This unique response means that a single Au nanorod-YSZ nanocomposite reacts differently to these gases and could be used to distinguish between H_2, NO_2, and CO in a system with an unknown combination of these gases. The thermal imaging data has issues distinguishing between the two reducing gases but with an improved S:N ratio, a more absolute picture will be possible.

Increasing the signal to noise for this measurements, in particular the energy harvesting data is simply a matter of increasing the aspect ratio of the rods such that they harvest a larger portion of the thermal energy from the tube furnace.

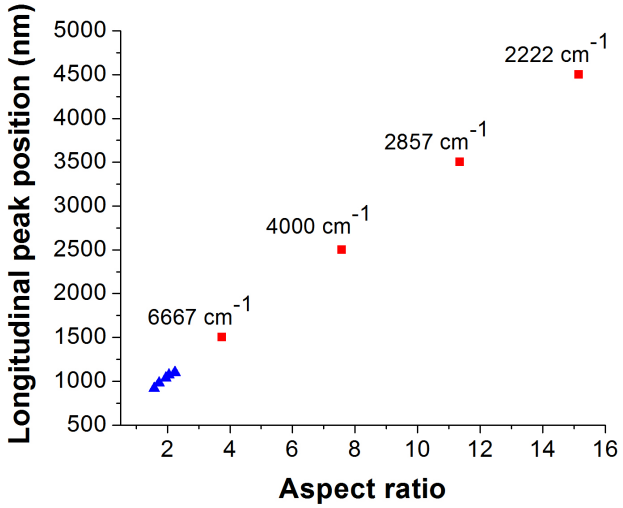

Figure 11. Longitudinal plasmon peak wavelength *vs.* nanorod aspect ratio for previously deposited samples as well as predicted plasmon peak positions obtained through linear extrapolation of the experimental data points.

At temperatures of 500°C and above, a large amount of the total thermal irradiance emanates from the near and mid infrared regions. While energy harvesting was demonstrated in the short

wavelength near infrared region where there is a minority of thermal photon counts. By increasing the length of the patterned nanorods, and therefore the aspect ratio, the longitudinal peak can be shifted further into the near infrared region if not into the mid infrared region, which would allow an improved S:N ratio. This characteristic is displayed in Figure 11, which plots the Au longitudinal plasmon peak position as a function of the nanorod aspect ratio. The first 5 data points in blue are from nanorod samples deposited using the same methods described earlier. In this figure each of the nanorods had the same width, and ranged in length from 70 nm to 100 nm, giving aspect ratios between 1.6 and 2.25. Aspect ratios ranging from 3.75 to 15.2 are realized by increasing the rod length to 165 and 667 nm, respectively, and performing a linear extrapolation of the experimental data points. On Figure 10, the red points pertain to the extrapolation of experimentally obtained longitudinal plasmon peaks between 1500 (6667cm^{-1}) and 4500 nm (2222 cm^{-1}), the latter of which is in an easily accessible region for FTIR spectrometers. Given the projected increase in S:N as well as the increased sensitivity of higher aspect ratio rods efforts were made to pattern such rods as well as to demonstrate the potential for development of not only the energy harvesting approach but also individual wavelengths that could be monitored to achieve not only high sensitivity but also selectivity.

5.0 Development of Single Wavelength Testing Bench

The proof of concept for the design of single wavelenth testing benches for the energy harvesting approach required an increase in the S:N from the previous measurements. The rods used for this demonstration are longer and have their peak plasmonic absorbance band in the near infrared, 1500nm. For comparison see Figure 12 and note that these rods have

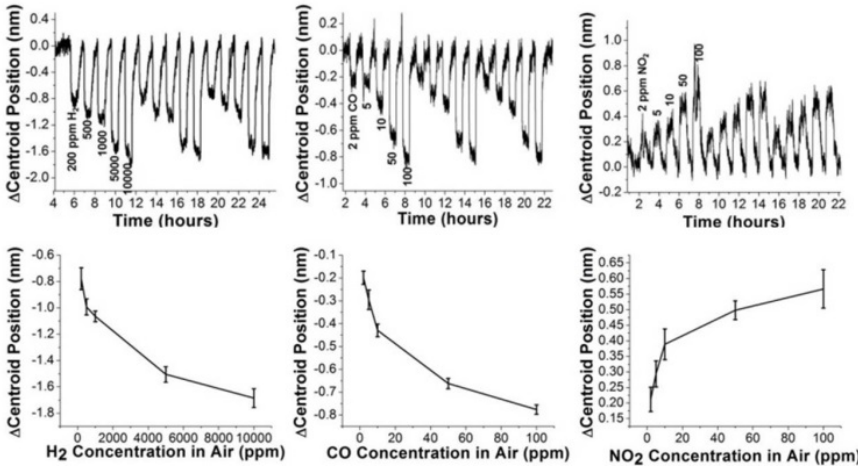

Figure 12. (Top Row) Gas sensing for the analyte gases: H_2, CO, and NO_2. (left) 200, 500, 1000, 5000, and 10000 ppm H_2 in air carrier gas. (middle) 2, 5, 10, 50, 100 ppm CO in air carrier gas. (right) 2, 5, 10, 50, 100 ppm NO_2 in air carrier gas. A spectral smoothing procedure was done followed by internal referencing to minimize baseline drift. The remaining baseline drift was corrected by removing linear drifts of 0.6 nm from the H_2 curve, 0.65 nm from the CO curve, and 0.5 nm from the NO_2 curve. The centroid position, or the center of mass of the absorbance curve, was used to track changes in the LSPR peak position.
(Bottom Row) Calibration plots for the H_2, CO, and NO_2 results shown in top row. Each data point averages 25 individual centroid positions from the Δcentroid vs. time graph to determine the average shift at each analyte gas concentration.

an aspect ratio near 4. These experiments and their analysis were completed and demonstrate the thermal energy harvesting enabled detection of emission gases (H_2, CO and NO_2). Due to the much larger amount of thermal energy radiation at these NIR wavelengths it is clear that using higher aspect ratio rods have improved the detection characteristics of this technique. Evidence of this is realized in that with the NIR absorbing nanorods data can be acquired every 20 seconds, whereas for nanorods with an aspect ratio of ~2 could only be acquired every 220 seconds . This 11 fold improvement is critical for future integration and application purposes as it will enable the necessary seconds level response times for combustion applications.

A single NIRQuest512 near-infrared spectrometer was used to measure NIR absorbance spectra as a function of both time and gas exposures for these sensing experiments. A mathematical replacement for a real-time reference was used to achieve improved baseline stability. Specifically, a method known as internal referencing was used to correct for baseline drift. Internal referencing requires selection of a single non-absorbing wavelength for a given sample and then using that wavelength to "re-normalize" the rest of the absorbance curve to the absorbance value at that wavelength. All optical sensing experiments, especially those at long time scales, benefit from having a real-time reference since light sources always have varying scan-to-scan intensity across the spectral range and also drift systematically. A technique such as internal referencing is a solution to this problem and can also work with the thermal harvesting technique since, similar to white light experiments, the intensity of thermal radiation produced by the furnace coils varies slightly around the furnace setpoint. This typically is not a significant problem in the thermal harvesting experiments, but provides extra stabilization to the technique over the 20 hour gas exposure experiments.

Gas sensing using the internal referencing procedure has been performed for different levels of H_2, CO, and NO_2 exposures up to maximum concentrations of 10000 ppm H_2, 100 ppm CO, and 100 ppm NO_2 in an air background and a 500°C sample temperature. The purge time for each analyte gas concentration in all of the sensing tests was 40 minutes. The absorption spectral data acquired from these experiments were used to determine the change in the LSPR centroid position as a function of time and gas exposure, Figure 12 (top), as well as the calibration curves determined from these exposures, Figure 12 (bottom). As expected both the H_2 and CO exposures show a characteristic blue shift in the LSPR while NO_2 exposures result in a red shift in the LSPR.

The calibration curves shown in Fig. 12 were made by averaging 25 centroid positions from each gas concentration and then plotting this averaged centroid shift vs. gas concentration for the three analyte gases. The average error bar percentages are 5.7% for H_2, 8.3% for CO, and 12.5% for NO_2. In all of the tests, the observed baseline noise is translated to the analyte gas response since it is noise coming from the detector as well as the light source. In the NO_2 test, since it has the smallest magnitude of peak shift between the three gases, the noise is more prevalent in the gas response and this is seen from the high error bar percentage.

Selectivity was characterized again using PCA analysis. Figure 13a shows the full spectrum PCA result that contains 413 wavelengths in the range of 1050nm-1700nm. Similar degrees of selectivity are achieved with the reduced wavelength approach (Fig. 13b) by selecting the wavelengths: 1350, 1410, and 1470. The wavelengths 1350 and 1470nm were selected to capture variance on either side of the LSPR absorbance peak, where the intensity at a given

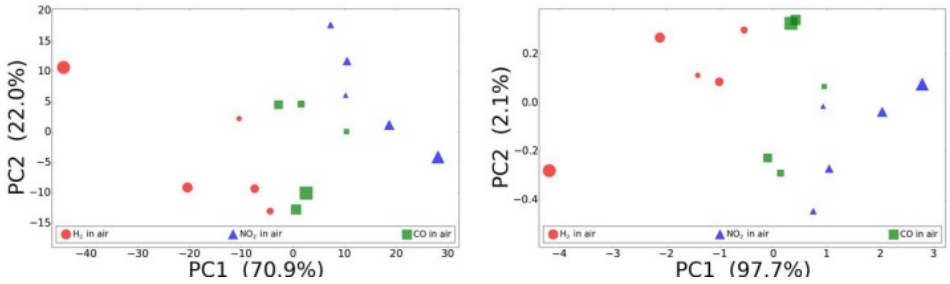

Figure 13. (a) Full spectrum PCA performed on wavelength range of 1050nm-1700nm. (b) Reduced wavelength PCA using wavelengths of 1350, 1410, 1470nm with similar selectivity as with the full spectrum PCA.

wavelength is shifting a particularly large amount from either a red or blue curve shift. The 1410nm wavelength was chosen due to its proximity to the plasmon peak position. Comparison of the gas-on and gas-off spectral overlays confirmed the choice of this wavelength subset. By reducing the wavelengths collected, we can reduce the amount of collected information significantly. By only requiring a small subset of wavelengths to be monitored while retaining the required detection limits and selectivity characteristics, the detection hardware can be simplified. NIR optical components such as sources and spectrometers already have low cost and are highly available due to demand from the telecommunications industry. AuNR-YSZ samples could be mounted on fiber optic cables and, combined with wavelength-dispersive multiplexing and detectors, would allow placement of a distributed network of optical plasmonic sensors in a combustion source. The NIR thermal energy harvesting approach along with multivariate analysis opens a pathway for miniaturization and integration of low-cost optical gas sensors.

6.0 Design of Packaging for Integrated Device

The current emission sensor packaging effort has been focused primarily on modeling and detailed analysis of the overall sensor prototype integrated into the UTC Aerospace Exhaust Gas Temperature (EGT) probe. The modeling and analysis consisted of temperature transient coefficients of thermal expansion analysis, and Computational Fluid Dynamics (CFD). The construction of the UTC Aerospace EGT probe allows for a flexible approach to the incorporation of the prototype emission sensor within the internal support structure of the probe. Therefore, the addition of the emission sensor does not adversely affect the EGT probes' functionality. The emission sensor packaging will be comprised of a high temperature optical fiber encased by a protective cladding. Additional sheathing will act as an interposer and be brazed to the fiber and existing internal spacers of the EGT probe creating a rigid support structure to reduce the risks associated with high temperature and engine vibrations. Material selection for the sensor package was selected based on the application temperature and the shroud design needed to stagnate the high velocity exhaust gas to both prevent erosion of the nano-composite coating and to ensure particulate evacuation from the sensing area. UTAS modeled the flow characteristics of the modified design. 3D printed, scaled down, prototypes were manufactured utilizing comparable materials to current design intent. Such prototypes allowed for higher precision CFD analysis and assisted with the details of the prototype design and integration. While extensive work

on the packaging design is still needed the theoretical designed package was outlined by UTAS within this program and would be compatible with the new alternative energy harvesting approach outlined above.

7.0 Extension – New Task Ag/AgOx – YSZ materials development

Recent work in the Carpenter lab has demonstrated the large plasmonic response of Ag/AgOx nanoparticles deposited on YSZ in the presence of changing redox gas conditions at temperatures ranging from 300-400C. The wavelength shift when switching from air to air-H_2 gas mixtures is nearly 200nm, by far the largest plasmonic response of any system to date under either ambient or harsh environment conditions. This collaborative work with the Ohodnicki work has continued through 2015 and the XPS results obtained by the NETL group match very well with the plasmonics results. A jointly authored manuscript has been nearly completed and will be submitted to a peer reviewed journal before December 2015.

8.0 Conclusions

In this work, we have shown for the first time that thermal radiation can be effectively harvested in the visible region of the electromagnetic spectrum by plasmonically active Au nanorods, and this method facilitates the collection of absorption spectra without the need for an external incident light source. Gas sensing results using this method of thermal energy harvesting have been performed and compared to white light gas sensing experiments which employ an external light source, and both show strong concentration dependence for the different analyte gases. Wavelength reduction has been performed using PCA methods, which significantly reduces the number of wavelengths that are required for acquiring effective sensing data, thus enabling the future use of individual wavelength detectors for the sensitive and selective detection of the target gases. A combination of both thermal harvesting and wavelength reduction has resulted in a new sensing paradigm, which will lead to a highly simplified sensor design that is low cost, reliable, and easier to integrate into emission gas application environments. Extension of these methods into the near and mid infrared regions was also completed and led to improved performance characteristics with regards to data acquisition times and S:N levels. The nanorod array assemblies used for these energy harvesting approaches have proven to have stability over several 50hr individual experiments with no appreciable degradation observed. It is noted that if the sensor array is exposed to ambient gaseous environments for significant periods of time the sample should undergo a pre-cleaning process which is simply exposure to 500-600^{o}C temperatures within an air environment to passivate the sample from adsorbed gaseous species. Integration challenges were designed and modeled by UTAS throughout this program and the combined thermal transfer and CFD analyses as well as the scaled 3D prototype designs all show promise as a viable housing for the newly developed plasmonics based energy harvesting chemical sensing paradigm developed within this program.

9.0 Index of Acronyms

PCA: principal component analysis
PC: principal components
YSZ: yttria-stabilized zirconia
XRD: x-ray diffraction
TEM: transmission electron microscopy
FWHM: full width half maximum
SVD: singular value decomposition
vs: versus
LSPR: localized surface plasmon resonance
AuNP: gold nanoparticle
AuNR: gold nanorod
PVD: physical vapor deposition
CCD: charge coupled device
Rf: radio frequency
sccm: standard cubic centimeters per minute
nm: nanometers
CNSE: Colleges of Nanoscale Science and Engineering
UTAS: United Technology Aerospace Systems
NETL: National Energy Technology Laboratory
XPS: x-ray photoelectron spectroscopy
CFD: computational fluid dynamics
FDTD: finite difference time domain
EGT: exhaust gas temperature
NIR: near infra-red
LSPR: localized surface plasmon resonance
S:N: signal to noise ratio
ppm : parts per million
ESEM: environmental scanning electrom microscopy
FIB: focused ion beam
PMMA: polymethyl methacrylate

10.0 References

[1] Rakic, A. D.; Djurišic, A. B.; Elazar, J. M.; Majewski, M. L. Optical Properties of Metallic Films for Vertical-Cavity Optoelectronic Devices. *Appl. Opt.* **1998**, 37, 5271–5283.

[2] S.E. Han and D.J. Norris, "Beaming thermal emission from hot metallic bull's eye," Optics Express, Vol. 18, No. 5, p. 4829 (2010).

[3] P. Nagpal, N.C. Lindquist, S.-H. Oh, D.J. Norris, "Ultrasmooth patterned metals for plasmonics and metamaterials," Science 325 (2009), p. 594.

[4] C. Lindquist, P. Nagpal, A. Lesuffleur, D.J. Norris, and S.-H. Oh, "Three-dimensional plasmonic nanofocusing," Nano Letters 10(4), 1369-1373 (2010).

[5] Kreiter, M., Oster, J., Sambles, R., Herminghaus, S., Mittler-Neher, S. and Knoll, W., "Thermally induced emission of light from a metallic diffraction grating, mediated by surface plasmons," Optics Communications 168, 117-122 (1999)

[6] K.-S. Lee and M. A. El-Sayed, *The Journal of Physical Chemistry B*, vol. 110, no. 39, pp. 19220-19225, Oct. 2006